ISSN 1027-5495. Functional Materials, 28, No.4 (2021), p. 676-682.
doi:https://doi.org/10.15407/fm28.04.676 

# Study on the effect of TiN deposition conditions on the features of texture formation in the two-layer system $TiN/Ni_{0.905}W_{0.095}$ suitable for creating paramagnetic substrates with cubic texture for 2G HTS superconductors

***T.V.Sukhareva, M.S.Sunhurov, V.A.Finkel, Yu.N.Shahov***

National Scientific Center "Kharkov Institute of Physics and Technology", National Academy of Sciences of Ukraine, 1 Akademicheskaya Str., 61108 Kharkov, Ukraine

*Received June 15, 2021*

The influence of TiN deposition conditions on the morphology and structure of the $TiN/Ni_{0.905}W_{0.095}$ two-layer system was studied. The effect of the simultaneous formation of a cubic texture both in the TiN coating and in the substrate based on the $Ni_{0.905}W_{0.095}$ paramagnetic alloy was detected using X-ray diffraction analysis. The composition $TiN/Ni_{0.905}W_{0.095}$ can be used as a substrate in the conductive architecture of 2G HTS to improve its critical current density.

**Keywords**: 2G HTS, superconductivity, cubic texture, TiN, Ni–W, buffer layer, paramagnetic substrate.

**Дослідження впливу умов осадження TiN на особливості текстуротворення у двошаровій системі $TiN/Ni_{0.905}W_{0.095}$ що придатна для створення парамагнітних підкладок з кубічною текстурою для 2G HTS надпровідників.** *Т.В.Сухарева, М.С.Сунгуров, В.А.Фінкель, Ю.М.Шахов*

Досліджено вплив умов осадження TiN на морфологію та структуру двошарової системи $TiN/Ni_{0.905}W_{0.095}$. За допомогою рентгеноструктурного аналізу було виявлено ефект одночасного утворення кубічної текстури як у підкладці на основі парамагнітного сплаву $Ni_{0.905}W_{0.095}$, так і у покритті TiN. Композиція $TiN/Ni_{0.905}W_{0.095}$ може бути використана як підкладка у струмопровідній архітектурі 2G HTS для покращення критичної щільності струму.

Исследовано влияние условий осаждения TiN на морфологию и структуру двухслойной системы $TiN/Ni_{0.905}W_{0.095}$. С помощью рентгеноструктурного анализа выявлено эффект одновременного образования кубической текстуры как в подложке на основе парамагнитного сплава $Ni_{0.905}W_{0.095}$, так и в покрытии TiN. Композиция $TiN/Ni_{0.905}W_{0.095}$ может быть использована в качестве подложки в токопроводящей архитектуре 2G HTS для улучшения критической плотности тока.

## *1. Introduction*

Research in the field of high-temperature superconductors of the second generation (2G HTS) based on YBCO textured films is of particular interest because it opens up new perspectives for creating coated conductors, which could operate in

high magnetic fields at the temperature of liquid nitrogen (77.4 K) [1–6]. First of all this refers to the transfer of electric current over long distances (in particular from the nuclear power plant to the consumer), the creation of powerful magnetic fields, etc [7, 8]. As known, the architecture of 2G HTS [9] with the crucial current density above $j_c \sim 10^6$ A/cm$^2$ at the liquid nitrogen temperature should consist of three main components [10–13]:

1. Metallic substrate (thin, flexible tape mostly of Ni–W alloys with different compositions);

2. Buffer layer/layers (oxides, nitrides, in particular TiN as seed layer);

3. Quasi-single-crystalline film of a high temperature superconductor $YBa_2Cu_3O_{7-\delta}$ ($T_c \sim 92$ K [14]) with a strongly reduced fraction of high angle grain boundaries.

Fabrication of high-$j_c$, biaxially aligned HTS films can be achieved due to epitaxial growth on rolling-assisted biaxially-textured substrates (RABiTS) [11, 15–18]. The texture (100)[100] of the metallic substrate is imparted to the superconductor by deposition of intermediate layers, which serve as chemical and structural buffers [19]. The conductive layer acts as an electric shunt to prevent the effect of thermal destruction of superconductor in the case of over-current; titanium nitride can be used as the main seed buffer layer in the complex architecture of 2G HTS [20–22].

Moreover, the metallic substrate must be in a paramagnetic state at low temperatures to reduce losses during ac current transport [23–25]. The property of paramagnetism is provided by increasing the concentration of tungsten in the $Ni_{(1-x)}W_x$ alloy to $x \sim 0.095$ [26, 27]. However, it hinders the formation of a cube texture (100)[100] due to a decrease in the stacking fault energy $E_s$ of the cold-rolled alloy. The $E_{sf}$ decreases with increasing the content of the alloying element in the alloy [28].

The main aim of this work is to find new ways to control properties of paramagnetic substrates based on the $Ni_{0.905}W_{0.095}$ alloy for creating high-temperature superconductors with high current-carrying capacity (2G HTS).

The following research program was implemented:

1. Experimental study of the effect of nitrogen pressure on the structural features of both components of the two-layer system $TiN/Ni_{0.905}W_{0.095}$ during titanium evaporation.

2. Experimental study of the influence of TiN deposition time on the structural features of the components of the $TiN/Ni_{0.905}W_{0.095}$ system at the optimal value of nitrogen pressure.

3. Experimental study of the influence of TiN deposition geometry on the structural features of both components of the $TiN/Ni_{0.905}W_{0.095}$ system.

4. Development of new ways to control the structure and properties of materials based on paramagnetic Ni–W alloys with a TiN coating.

## 2. Materials and methods

Preparation of substrates was carried out according to the scheme, which includes the following steps [29, 30]: 1) synthesis of a paramagnetic alloy $Ni_{0.905}W_{0.095}$; 2) production of thin-layer tapes; 3) high-temperature treatment of NiW tapes; 4) deposition of titanium nitride on the surface of a NiW tape; 5) XRD analysis of obtained samples.

The initial materials for obtaining the Ni–W alloys were Ni and W powders with 99.98–99.99 % purity (by metallic impurities). The following methods were used to remove gaseous impurities (the main impurity is oxygen in the form of nickel and tungsten oxides): 1) heat treatment at temperatures ~ 850°C to clean Ni powder; 2) high-temperature treatment (1000–1200°C) in the Ar + 4 % $H_2$ gaseous mixture flow to clean W powder. The paramagnetic alloy was synthesized by means of powder metallurgy in a deep vacuum ($p \sim 10^{-6}$ Torr) at $T = 1200$°C for $t = 4$ h.

Obtained ingots were rolled up to 50–100 μm thickness at room temperature to make metallic tapes. The total degree of cold-rolling deformation was about 95 %. The last operation was high-temperature annealing of the tapes at $T = 1150$°C for $t = 2$ h.

Thin layers of titanium nitride (TiN) on the surface of Ni — 9.5 at % W tapes were deposited by the ion-plasma method [31]. Specific parameters of the TiN buffer layer deposition varied within the following ranges: negative substrate potential $U = 50$–$300$ V; arc current $I = 80$ A; substrate temperature $t_s \sim 450$°C; nitrogen pressure in the chamber $p_N = 1.2$–$6.2 \cdot 10^{-2}$ Torr; deposition time $\tau_{TiN} = 0$–$900$ s.

XRD analysis (filtered Cu Kα radiation) was carried out for the following tasks: determination of the phase composition of the $Ni_{0.905}W_{0.095}$ substrate and TiN coating; de-

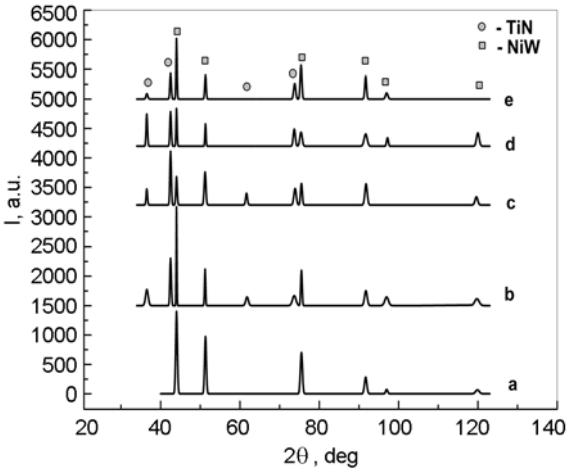


Fig.1.Set of diffraction patterns of the system TiN/$Ni_{0.905}W_{0.095}$ for the experimental series at different pressures ("shadow"): a) $Ni_{0.905}W_{0.095}$ without coating; b) 1.2, c) 1.8, d) 2.8, e) $3.8 \cdot 10^{-2}$Torr.

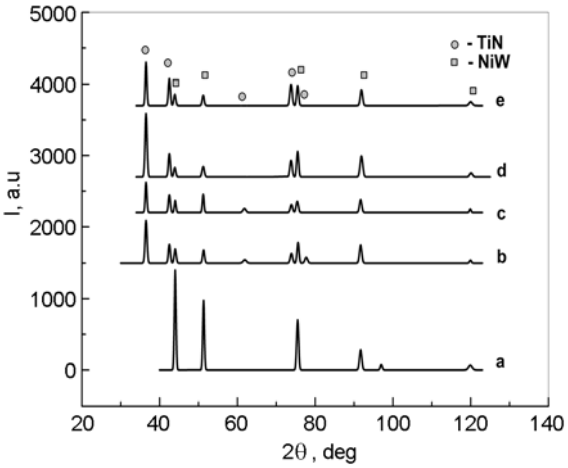


Fig.2. Set of diffraction patterns of the system TiN/$Ni_{0.905}W_{0.095}$ for the experimental series at different pressures ("face"): a)$Ni_{0.905}W_{0.095}$ without coating; b) 1.2, c) 1.8, d) 2.8, e) $3.8 \cdot 10^{-2}$Torr.

termination of lattice parameters; analysis of the texture of the substrate and the coating [31]; determination of the TiN coating thickness [32–34].

To determine the TiN lattice parameter, the diffraction line (220) was analyzed. Its position was measured with an accuracy of $\Delta 2\theta = 0.01$ deg. The diffraction line profile was approximated as a convolution of two Gaussian functions (parameter $R^2 = 0.95$). The lattice constants calculated for $K\alpha 1$ and $K\alpha 2$ lines coincide with an accuracy of $\Delta a = 0.0001$ Å.

The method for determining the thickness of the TiN layer is based on the absorption of X-ray radiation. The intensity of the beam reflected from the crystal plane ($hkl$) of a sample with the coating thickness $h$ is as follows:

$$I_h = I_0 \cdot \exp(-2h_{TiN} \cdot \mu_{TiN}/\sin\theta), \qquad (1)$$

where $I_h$ is the intensity of the beam reflected from the substrate with coating; $I_0$ is the intensity of the beam reflected from the substrate without coating; $h_{TiN}$ is coating layer thickness; $\mu_{TiN}$ is the linear absorption coefficient of the coating material; $\theta$ is the Bragg angle.

Equation (1) and mathematical modeling of the relative intensity of some X-ray reflections, in our case, from the cubic plane ($h00$) of the Ni–W substrate, makes it possible to determine the coating thickness $h_{TiN}$ with an accuracy of about 10 %.

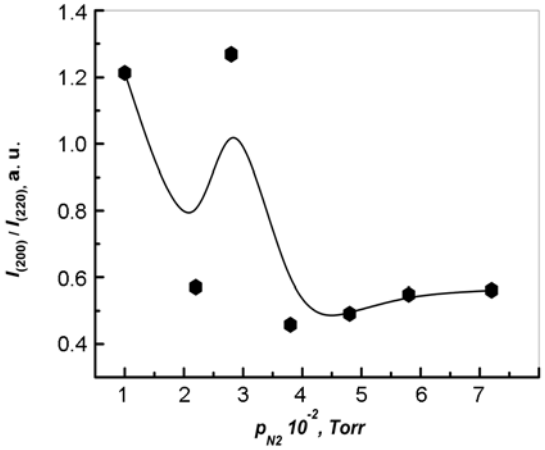


Fig. 3. Values of the ratio $I_{(200)}/I_{(220)}$ for the $Ni_{0.905}W_{0.095}$ substrate after TiN deposition.

## 3. Results and discussion

In the present study, the TiN coating was applied to the front ("face") and back ("shadow") sides, i.e. outside the line of the cathode ray hitting the $Ni_{0.905}W_{0.095}$ substrate. Two series of experiments were carried out:

— The deposition of TiN at a constant time $t_{TiN} = 5$ min in a wide range of pressures of nitrogen $p_N = 1.2–6.2 \cdot 10^{-2}$ Torr.

— The deposition of TiN at a constant (optimal) $N_2$ pressure of nitrogen for different times $\tau_{TiN} = 1–3$ min.

Fig. 1 and Fig. 2 present a set of diffraction patterns of the experimental series of the TiN/$Ni_{0.905}W_{0.095}$ system at different

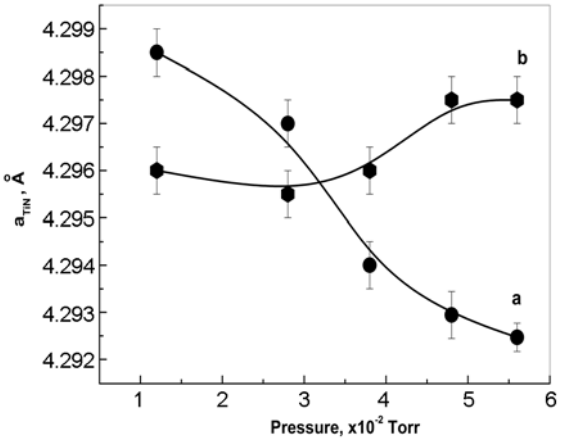


Fig. 4. Lattice parameters of the TiN coating deposited onto both sides of the $Ni_{0.905}W_{0.095}$ substrate at different pressures of nitrogen depending on the coating geometry: a) face; b) shadow.

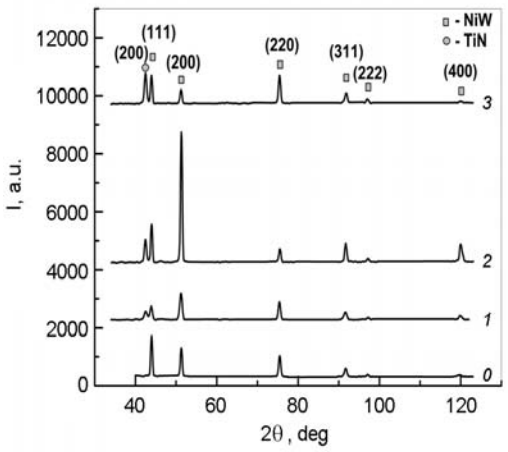


Fig. 5. XRD patterns of $Ni_{0.905}W_{0.095}$ alloy tapes with TiN coating ("Face") at $p_N$ = $1.8 \cdot 10^{-2}$ Torr in the range of 0–3 min (from bottom to top).

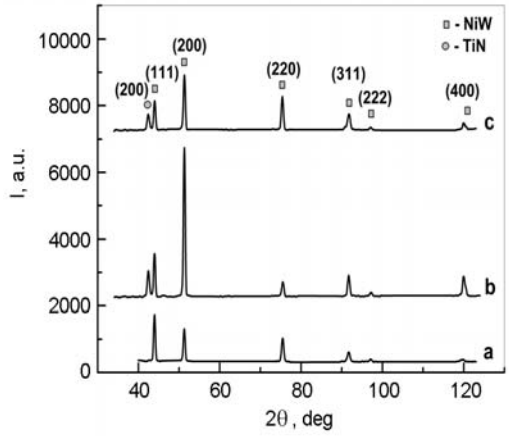


Fig. 6. XRD patterns of $Ni_{0.905}W_{0.095}$ alloy tapes with TiN coating obtained at optimized conditions ($p_N = 1.8 \cdot 10^{-2}$ Torr, $t$=2 min at different coating geometry a) original sample, b) face, c) shadow.

pressures for both face and shadow deposition geometries. There are two systems of diffraction lines, which belong to the FCC lattice of the $Ni_{0.905}W_{0.095}$ alloy and the TiN lattice of the NaCl type. As the pressure of nitrogen increases, textures of the substrate and coating change.

Naturally, an increase in $p_N$ leads to an increase in the intensity of TiN diffraction lines, but at the same time, there is a tendency to redistribution of the intensities of diffraction lines for the $Ni_{0.905}W_{0.095}$ subsystem.

The Fig. 3 clearly shows a considerable increase in the intensity of lines from Ni–W "cubic" plane $I_{(200)}$ at $p_N \sim 1.8 \cdot 10^{-2}$ Torr, indicating the sharpening of the cubic texture of the metallic component. The ratio of intensities of "cubic" $I_{(200)}$ and "diagonal" $I_{(220)}$ diffraction lines was chosen as a "texture parameter".

The Fig. 4 shows the dependences of TiN lattice constant a TiN on the pressure of $N^2$ for different coating deposition geometries.

As can be seen, in the case of the "shadow" geometry, the curve *a* weakly depends on the $p_N$, while for the "face" geometry, the curve *b* decreases monotonically over the entire range of nitrogen pressures. Dynamics of the change in the TiN lattice parameter during the formation of the crystalline phase in the coating can be associated with the change in the flux densities of titanium and nitrogen atoms, depending on the deposition geometry.

The above data (see Fig. 1–4) give reason to believe that at pressures $p_N \sim 1.8 \cdot 10^{-2}$ Torr, the most favorable conditions appear for the formation of cubic texture of the substrate in the $TiN/Ni_{0.905}W_{0.095}$ system.

The evolution of the diffraction pattern depending on the TiN deposition time at optimized $p_N = 1.8 \cdot 10^{-2}$ Torr = *const* is shown in Fig. 5. As the deposition time $\tau_{TiN}$ increases up to 2 min, in other words, as the coating thickness increases, the relative intensity of diffraction lines of the (*h*00) type increases, while the intensities of reflections from the diagonal (*hk*0) and other FCC lattice planes decrease. This behavior indicates a qualitatively significant enhancement of the degree of cubic texture in the tape made of the $Ni_{0.905}W_{0.095}$ paramagnetic

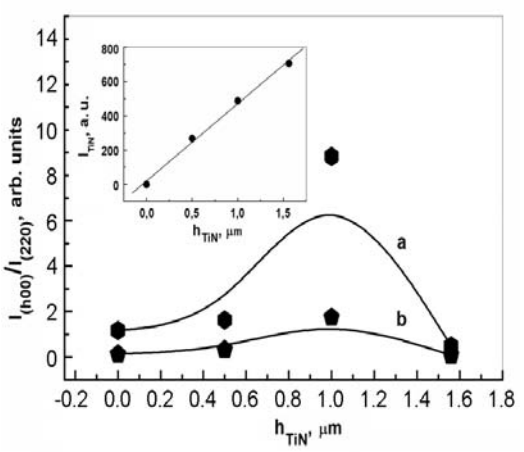


Fig. 7. Dependences of $I_{(h00)}/I_{(220)}$ ratio from $Ni_{0.905}W_{0.095}$ substrate on the TiN thickness. Inset: Dependence of $I_{(200)}(h_{TiN})$ for titanium nitride coating: a) face, b) shadow.

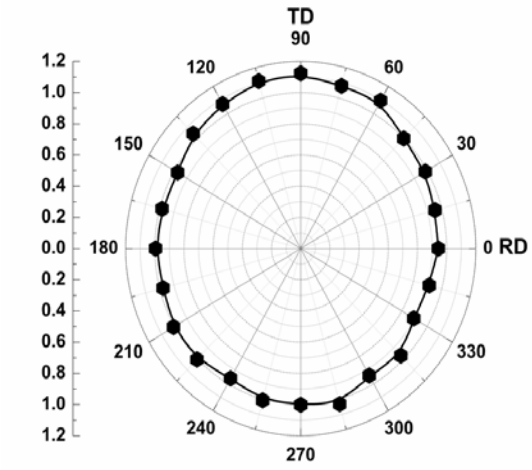


Fig.8. Circular diagram of (200) plane for the TiN coating.

alloy. According to Fig. 6, the diffraction patterns of the TiN/NiW systems obtained with different deposition geometries of TiN indicate the texture enhancement effect, which is more evident for the geometry of the "face" coating.

The Fig. 7 shows the dependency of texture parameter for $Ni_{0.905}W_{0.095}$ versus thickness of TiN coating at $p_N = 1.8 \cdot 10^{-2}$ Torr , calculated by the eq. (1). As can be seen, there is a strong maximum for $h_{TiN} \sim 1$ μm. The process of cubic texture formation is also observed in the TiN layer. This is evidenced by the presence of only the (200) TiN diffraction line from the cubic plane of the TiN lattice. The inset in Fig. 7 indicates that the intensity $I_{(200)}$ from TiN monotonically increases.

To determine small variations in texture in the $TiN/Ni_{0.905}W_{0.095}$ system, the pie chart algorithm was used as an addition to the classical methods. This method is based on the construction and analysis of diagrams of the angular distribution of the intensity from crystallographic planes. To study the density of the (*hkl*) plane normals in different directions, the sample must be rotated by an angle φ relative to the normal to its surface.

The well-known statistical method $\chi^2$ was chosen as a criterion for the validity of the initial hypothesis about the realization of an ideal cubic texture. To calculate it, $n = 23$ degrees of freedom were considered. Of course, in the case of forming an ideal cubic texture, the value of "Chisquare" tends to be zero.

As an illustration, Fig. 8 shows a circular diagram from (200) planes for a TiN coating with $h_{TiN} \sim 1$ μm, where the texture

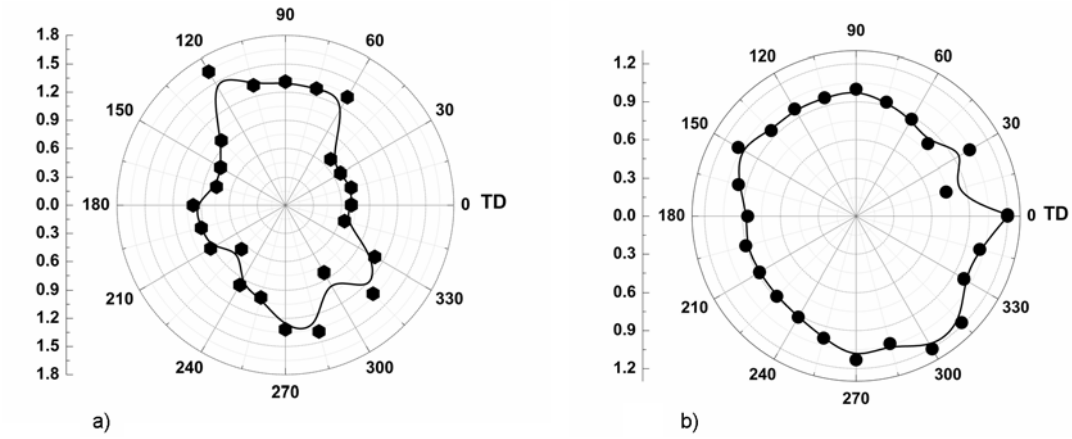


Fig. 9. Circular diagram of (200) plane from a) original tape based on the $Ni_{0.905}W_{0.095}$ alloy and b) subsystem $Ni_{0.905}W_{0.095}$ of the two-layer composition "substrate NiW — coating TiN".

effects in the substrate are most pronounced. Fig. 9 shows circular diagrams from (200) planes of the $Ni_{0.905}W_{0.095}$ subsystem before (Fig. 9a) and after coating (Fig. 9b) at optimized parameters: $\tau_{TiN}$ = 2 min, $p_N = 1.8 \cdot 10^{-2}$ Torr, $h_{TiN} \sim 1$ μm.

It is worth to mention that for crystals having a cubic symmetry, the polar absorption tensor does not depend on the direction. Thus, any change in the intensity of the diffracted beam can be solely attributed to the processes of texture formation occurring in a two-layer system "substrate — coating". One can see from the graphs above that the deposition of the TiN coating leads to the improvement of the cubic texture ($\chi_{tape} = 0.11 \rightarrow \chi_{coated} = 0.07$) in the metal component (Ni–W) of the two-layer system $TiN/Ni_{0.905}W_{0.095}$ as well as to the formation of a strong texture in the coating ($\chi_{TiN} = 0.005$).

The subject of discussion in this paper is a set of observed effects associated with the peculiarities of the formation of a cubic texture in the thin-film system $TiN/Ni_{0.905}W_{0.095}$ (see Fig. 3–9):

A qualitative change in the dependencies of a crystal lattice parameter of titanium nitride on the nitrogen pressure with a change in the "geometry" of deposition during the experiment.

A significant increase in the cubic orientation in the $Ni_{0.905}W_{0.095}$ metallic layer of the $TiN/Ni_{0.905}W_{0.095}$ thin-layer system.

Formation of a sharp cubic texture of the TiN buffer layer in the $TiN/Ni_{0.905}W_{0.095}$ system.

The revealed differences in the dependences of the lattice parameters of titanium nitride may be caused by differences in the mechanisms and kinetics of the phase formation of TiN titanium nitride when Ni–W is deposited on different sides of the Ni–W tape. The dependence for the "front" side reflects an increase in the proportion of atoms with low atomic radius. For the "shadow" side, the dependence reflects a mechanical decrease in the titanium ion flux density due to deposition on the opposite side of the substrate. It cannot be ruled out that the order of the reaction between the Ti and N ions may change.

The set of data shown in Figs. 5–7 clearly indicates the processes of texture formation in the substrate based on the $Ni_{0.905}W_{0.095}$ paramagnetic alloy due to the effect of the TiN layer. This is clearly confirmed by the change of the intensity distribution from $(200)_{NiW}$ crystal plane as shown in the Fig. 9.

The effect of an anomalous increase in the degree of a cubic texture in the substrate, as well as the formation of a biaxial texture in the coating, is obviously associated with the process of reorientation of crystallites of both components of the $TiN/Ni_{0.905}W_{0.095}$ system under the influence of interfacial stresses arising at the interface of materials with different lattice parameters.

## 4. Conclusion

Methods have been developed to control the architecture of the $TiN/Ni_{0.905}W_{0.095}$ two-layer system, based on the change in the nitrogen pressure during titanium evaporation, the deposition time, and the geometry of the coating.

The conditions for creating two-layer "substrate — coating" compositions are optimized, which provide the possibility of obtaining sharp cubic texture in the TiN coating deposited on the tape based on the $Ni_{0.905}W_{0.095}$ paramagnetic alloy.

The main result of the work is the experimental detection of correlated formation of a cubic texture in both components of the $TiN/Ni_{0.905}W_{0.095}$ two-layer system, which should provide a significant increase in the critical current density of 2G HTS coated conductors.

## References


1. J.G.Bednorz, K.A.Muller, *Z. Physik B — Condensed Matter.*, **64**, 189 (1986). https://doi.org/10.1007/BF01303701
2. M.W.Rupich, X.Li, C.Thieme et al., *Supercond. Scien. Techn.*, **23**, 014015 (2009). https://doi.org/10.1088/0953-2048/23/1/014015
3. M.Paranthaman, C.Park, X.Cui et al., *J. . Mater. Res.* **15**, 2647 (2000). https://doi.org/10.1557/JMR.2000.0379
4. M.W.Rupich, U.Schoop, D.T.Verebelyi et al., *IEEE Trans. Appli. Supercond.,* **13**, 2458 (2003). DOI:10.1109/TASC.2003.811820.
5. D.Larbalestier, A.Gurevich, D.Feldmann et al., *Nature*, **414**, 368 (2001). https://doi.org/10.1038/35104654
6. W.V.Hassenzahl, *IEEE Trans, Appli. Supercond.*, **11**, 1447 (2001). DOI:10.1109/77.920045
7. M.Wilson, Superconducting Magnets, Clarendon, Oxford (1983).
8. T.Pyon, T.E.Gregory, *IEEE Trans.Appl. Supercond.*, **11**, 3688 (2001). DOI:10.1109/77.919865

9. Y.Shiohara, T.Taneda, M.Yoshizumi, *Jpn. J. Appl. Phis.*, **51**, 010007 (2012). https://doi.org/10.1143/JJAP.51.010007
10. A.P.Malozemoff, S.Annavarapu et al., *Supercond. Sci. Technol.*, **13**, 473 (2000). https://doi.org/10.1088/0953-2048/13/5/308
11. A.Goyal. Epitaxial Superconductors on Rolling-Assisted-Biaxially-Textured-Substrates (RABiTS). In: Goyal A. (eds), Second-Generation HTS Conductors. Springer, Boston, MA (2005). https://doi.org/10.1007/0-387-25839-6_2
12. E.D.Specht, A.Goyal et al., *Supercond. Sci. Technol.*, **11**, 945 (1998). https://doi.org/10.1088/0953-2048/11/10/009
13. M.Paranthaman, A.Goyal, F.List et al., *Physica C: Superconductivity*, **275**, **3–4**, 266272 (1997). https://doi.org/10.1016/S0921-4534(96)00713-7.
14. M.K.Wu et al., *Phys. Rev. Lett.*, **58**, 908 (1987). https://doi.org/10.1103/PhysRevLett.58.908
15. J.Eickemeyer, D.Selbmann, R.Huhne et al., *Appl. Phys. Lett.*, **90**, 012510 (2007). https://doi.org/10.1063/1.2429905
16. D.P.Norton, A.Goyal, J.D.Budai et al., *Science*, **274**, 755 (1996). DOI:10.1126/science.274.5288.755
17. Y.Iijima, K.Onabe, N.Futaki et al., *J. Appl. Phys*, **74**, 1905 (1993). https://doi.org/10.1063/1.354801
18. A.Goyal, D.P.Norton, J.D.Budai et al., *Appl. Phys. Lett.*, **69**, 1795 (1996). https://doi.org/10.1063/1.117489
19. R.Huhne, D.Selbmann, J.Eickemeyer et al., *Supercond. Sci. Technol.*, **19**, 169 (2006). https://doi.org/10.1088/0953-2048/19/2/003
20. R.Huhne, S.Fahler, B.Holzapfel, *Appl. Phys. Lett.*, **85**, 2744 (2004). https://doi.org/10.1063/1.1802385
21. R.Gartner, R.Huhne, J.Engelmann et al., *IEEE Trans. Appl .Supercond.*, **21**, 2920 (2010). DOI:10.1109/ TASC.2010.2080657
22. K.Guth, R.Huhne, V.Matias et al., *IEEE Trans. Appl. Supercond.*, **19**, 3447 (2009). https://doi.org/10.1109/ TASC.2009.2019249
23. J.R.Thompson, A.Goyal, D.K.Christen et al., *Physica C: Superconductivity*, **370**, 169 (2002). https://doi.org/10.1016/S0921-4534(01)00937-6
24. U.Gaitzsch, J.Hanisch, R.Huhne et al., *Supercond. Scien. Techn.*, **26**, 085024 (2013). https://doi.org/10.1088/0953-2048/26/8/085024
25. S.V.Subramanya, J.Eickemeyer, L.Schultz et al., *Scr. Mater.*, **50**, 953 (2004). https://doi.org/10.1016/j.scriptamat.2004.01.004
26. R.Huhne, J.Eickemeyer, V.S.Sarma et al., *Supercond. Sci. Technol.*, **23**, 03401 (2010). https://doi.org/10.1088/0953-2048/23/3/034015
27. V.V.Derevyanko, M.S.Sungurov, T.V.Sukhareva et al., *Phys. Solid State*, **60**, 1930 (2018). DOI:10.1134/S1063783418100062
28. F.A.Mohamed, *Mater. Scie. Engin.*, **38**, 73 (1979). https://doi.org/ 10.1016/0025-5416(79)90034-X.
29. V.A.Finkel, A.M.Bovda, V.V.Derevyanko et al., *Functional Materials*, **19**, 109 (2012).
30. V.A.Finkel, V.V.Derevyanko, M.S.Sungurov et al., *Functional Materials*, **20**, 103 (2013). DOI:10.15407/fm20.01.103
31. I.I.Aksenov, V.M.Khoroshikh, N.S.Lomino et al., *IEEE Trans. Plasma Sci.*, **27**, 1026 (1999).
32. M.S.Sungurov, V.V.Derevyanko, S.A.Leonov et al., *Tech. Phys. Lett.*, **40**, 797 (2014). https://doi.org/10.1134/S1063785014090314
32. H.Friedman, L.S.Birks, *Review of Scientific Instruments*, **17**, 99 (1946). http://dx.doi.org/10.1063/1.1770449
33. I.Tomov, S.Vasiliev, *Solid State Phenomena*, **130**, 43 (2007). http://dx.doi.org/10.4028/www.scientific.net/SSP.130.43
34. V.A.Finkel, T.V.Sukhareva, M.S.Sungurov, *Low Temp. Phys.*, **46**, 594 (2020). https://doi.org/10.1063/10.0001241.